

THE POWER OF NEGATIVE ZERO: DATATYPE CUSTOMIZATION FOR QUANTIZED LARGE LANGUAGE MODELS

Yuzong Chen^{1*} Xilai Dai^{1*} Chi-chih Chang^{1*} Yash Akhauri¹ Mohamed S. Abdelfattah¹

ABSTRACT

Large language models (LLMs) have demonstrated remarkable performance across various machine learning tasks, quickly becoming one of the most prevalent AI workloads. Yet the substantial memory requirement of LLMs significantly hinders their deployment for end users. Post-training quantization (PTQ) serves as one of the most hardware-efficient methods to mitigate the memory and computational demands of LLMs. Although the traditional integer (INT) datatype has received widespread adoption in PTQ methods, floating-point (FP) quantization has emerged as a viable alternative thanks to its effectiveness in fitting LLM numerical distributions. However, the FP datatype in sign-magnitude binary representation contains both positive and negative zero, which constrains its representation capability, particularly under low precision (3 and 4 bits). In this paper, we extend the basic FP datatype to perform **Redundant Zero Remapping (RaZeR)**, which remaps the negative zero FP encoding to a set of pre-defined *special values* to maximally utilize FP quantization encodings and to better fit LLM numerical distributions. Through careful selection of special values, RaZeR outperforms conventional asymmetric INT quantization while achieving high computational efficiency. We demonstrate that RaZeR can be seamlessly integrated with quantization algorithms for both weights and KV-cache, including advanced methods with clipping and transformations, and consistently achieve better model accuracy. Additionally, we implement a fast GEMV kernel with fused dequantization that efficiently converts the 4-bit RaZeR value to FP16 through novel bit-level manipulation. On modern GPUs, our evaluation shows that RaZeR improves the GEMV speed by up to $7.56\times$ compared to the FP16 implementation, while achieving up to $2.72\times$ speedup in the LLM decoding throughput. Our code is available at <https://github.com/abdefattah-lab/RaZeR>

1 INTRODUCTION

Large Language Models (LLMs) are rapidly increasing in adoption, from chat-bots (Touvron et al., 2023; OpenAI), to coding assistants (Hui et al., 2024; Guo et al., 2024a), and agentic workflows (Wu et al., 2023). Thanks to their superiority in language modeling tasks and their emergent reasoning capabilities, LLMs are poised to become one of the most important, yet challenging computing workloads of our time. LLMs are computationally very heavy workloads, even at inference time, requiring the memory loading of tens or hundreds of billions of parameters, and resulting in proportionally large computations. With increased adoption, the high memory and compute overheads of LLMs are further exacerbated, spurring many research avenues into effective compression methods for LLMs to improve their efficiency and performance.

^{*}Equal contribution ¹Cornell University. Correspondence to: Yuzong Chen <yc2367@cornell.edu>, Xilai Dai <xd44@cornell.edu>, Chi-chih Chang <cc2869@cornell.edu>, Mohamed S. Abdelfattah <mohamed@cornell.edu>.

Post-Training Quantization (PTQ) continues to be among the most hardware-friendly LLM compression methods, especially in reducing the memory footprint. While compute performance is increasing in importance as well for high-batch optimized inference servers (Zhu et al., 2024), the memory footprint of LLM weights and KV-cache continues to be the key motivation for quantization. There are many prior works that attempt to quantize the weights (Dettmers et al., 2024; Lin et al., 2024; Zhao et al., 2024; Shao et al., 2024; Chee et al., 2023; Tseng et al., 2024; Frantar et al., 2022; Chen et al., 2024; Kim et al., 2024), and KV-cache (Liu et al., 2024; Hooper et al., 2024; Kang et al., 2024) at sub-8-bit precision. Many of these works have used integer datatypes thanks to its simplicity and compute friendliness. However, integer datatypes do not fit the numerical distributions of LLMs well that typically resemble a long-tailed Normal distribution. This has motivated completely custom codebook-based quantization schemes such as normal-float (NF4) (Dettmers et al., 2023), student-float (SF4) (Dotzel et al., 2024), and QuIP (Chee et al., 2023).

At 3- and 4-bit quantization, the datatype choice has a big impact on quantization accuracy and performance. On one

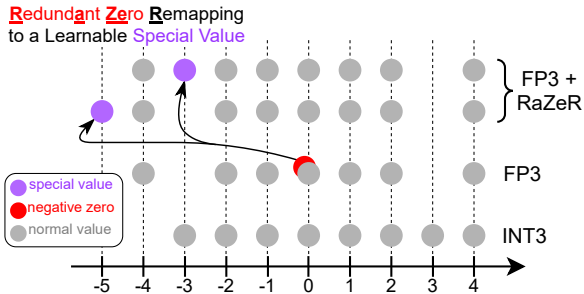


Figure 1. Floating point (FP) datatypes have redundant encodings for the zero value as it can be represented either as $+0$ or -0 . We remap the redundant zero to a learnable “special value” per quantization group to significantly decrease the LLM quantization error at 3 and 4 bits, for both weight and KV-cache quantization.

extreme, integer quantization is simple and can be used for both storage and computation but suffers from lower accuracy. At the other extreme, codebook quantization achieves the best accuracy at the cost of additional memory overhead to store the codebooks, and notable computational overhead to cast to a compute-capable datatype (Chen et al., 2024). This motivates the investigation of other hardware-friendly datatypes such as floating-point (FP), which strikes a reasonable balance between accuracy and performance. Furthermore, many of the recently-announced GPUs contain native support for FP4/FP6, such as Nvidia Blackwell B200 (NVIDIA, a;b) and AMD Instinct MI350X (AMD). As Figure 2 shows, the FP datatype also adheres better to the Normal distribution within LLMs, especially closer to the center of the distribution, contributing to their higher accuracy compared to integer formats.

In this paper, we build on FP4 and FP3 datatypes¹, specifically, the E2M1 and E2M0 variants. We propose **Redundant Zero Remapping (RaZeR)** to remap the FP negative zero encoding to a *special value*, optimized to decrease quantization error. Indeed, conventional FP datatypes include encoding for both $+0$ and -0 (Open Compute Project) due to the inherent sign-magnitude binary representation. This wasted encoding makes little difference for FP8 or higher bit-width formats because it signifies less than 0.4% of the possible quantization levels. However, at 4 and 3 bits, this wasted encoding constitutes a significant fraction of the quantization levels, 6.25% and 12.5% respectively. This greatly hinders the accuracy of FP4 and FP3 quantization for LLMs, and motivates our proposed RaZeR datatype that can reuse this redundant encoding to customize the FP datatype for each group of quantized numbers. By replacing -0 with a special value for each group of numbers, RaZeR datatypes have built-in adaptability to nuanced differences in numer-

¹FP datatypes are represented by their number of exponent (E) and mantissa (M) bits. For example, E2M1 is an FP4 variant with 1 sign bit, 2 exponent bits, and 1 mantissa bit.

ical distributions across an LLM. Furthermore, we select the special value with an explicit objective to decrease the quantization error in a fast calibration step, making RaZeR a practical way to customize numerical datatypes during quantization.

RaZeR is compatible with most existing LLM quantization methods, because it requires only a datatype change, and does not dictate a certain quantization algorithm. An additional special value calibration step is added to existing quantization algorithms. In fact, we combine RaZeR with weight-only quantization methods such as AWQ (Lin et al., 2024) and OmniQuant (Shao et al., 2024), in addition to KV-cache quantization methods like KCVT (Kang et al., 2024) and KIVI (Liu et al., 2024), demonstrating consistent accuracy improvements. The special value is treated like other quantization parameters (scaling factors and zero points), and has minimal encoding overhead—only 2 bits for each group of 128 numbers. Additionally, we implement an efficient GPU kernel to make RaZeR a drop-in replacement for existing quantized LLMs, achieving competitive performance to integer formats on currently-available GPUs. On upcoming and future GPUs, with native FP4/FP3 support, we anticipate even higher performance gains, and we hope that our work will provide a compelling argument to add hardware support for special value decoding in low-precision FP datatypes. Our contributions are summarized as follows:

1. We propose RaZeR: the remapping of redundant negative zero encoding in FP4 and FP3 to optimized special values to take the advantage of an additional quantization level for reducing LLM quantization error.
2. We combine RaZeR with four quantization algorithms including both weight and KV-cache quantization, showing consistent improvements in perplexity and downstream task accuracy, including long-context evaluation tasks.
3. We implement RaZeR end-to-end on current GPUs, achieving up to $7.56\times$ faster GEMV performance and $2.72\times$ higher LLM decoding throughput, compared to the FP16 implementation.

2 BACKGROUND

LLMs suffer from a very large memory footprint, and in many cases, especially low-batch inference, their compute latency is severely memory-bound. This is due to both the model size and the size of the KV-cache. This has motivated low-bit-width quantization to reduce the memory footprint and memory bandwidth, enabling LLM deployment on devices with less memory, and speeding up inference.

2.1 Quantization Basics

Quantization converts FP32 or FP16 operands to much lower bit widths, typically ≤ 8 bits. To perform asymmetric quantization, a tensor X is approximated to \tilde{X} as follows:

$$\tilde{X} = clamp(\lfloor \frac{X}{s} \rfloor + z, 0, 2^n - 1) \quad (1)$$

$$s = \frac{\alpha \max(X) - \beta \min(X)}{2^n - 1}, \quad z = -\lfloor \frac{\beta \min(X)}{s} \rfloor \quad (2)$$

where s , z , and n are the quantization parameters: scale factor, zero point, and number of bits in the quantized values respectively. α and β are optional quantization parameters to determine the clipping range that can simply be set to ones, an empirically-derived value (Choi et al., 2018), or learned during quantization-aware fine-tuning (Shao et al., 2024). $\lfloor \cdot \rfloor$ is the round-to-nearest function that maps a rescaled floating-point value to a quantized low-bit value.

This mapping introduces quantization error (ϵ_q) that is commonly quantified using a mean-squared error (MSE) or Kullback-Liebler divergence (KL):

$$\epsilon_q^{MSE} = \sum_i (X_i - \tilde{X}_i)^2, \quad \epsilon_q^{KL} = \sum_i X_i \log \frac{X_i}{\tilde{X}_i} \quad (3)$$

The quantized numerical format dictates the possible values for \tilde{X} , and therefore directly affects the quantization error. Integer datatypes (Wu et al., 2020) provides equally-spaced quantization values, making their compute circuitry simple and efficient. However, the numerical distribution within LLMs (and DNNs more generally) typically follow Normal distribution, with most of the values clustered around zero, resulting in high quantization error for integer datatypes that treat all values equally. This has motivated a number of investigations into new numerical representations that explicitly conform to the Normal distribution such as NF4 (Dettmers et al., 2023) and SF4 (Dotzel et al., 2024). With non-uniformly-spaced values, there are more quantization options surrounding the peak of the Normal distribution where most values are clustered, thus decreasing ϵ_q , at the expense of sparser quantization options at the tail of the distribution. Despite their superior performance, these formats store the quantized values as lookup indices, hence cannot be directly used for computing and need up-casting into a format such as FP16 (Guo et al., 2024b) for calculation.

Compared to lookup-based formats, mini floating-point datatypes such as FP4 and FP3 (Open Compute Project) strike a good balance between minimizing quantization error and compute efficiency. In addition, many new GPUs include native support for FP6 and FP4 such as Nvidia Blackwell B200 (NVIDIA, a;b) and AMD MI350 (AMD). In this paper, we extend FP4 and FP3 formats with optimized special values (as detailed in Section 4) to boost their accuracy without compromising compute performance.

2.2 Quantization Algorithms

Depending on the operands to be quantized, exiting LLM quantization algorithms can be classified into two categories: (1) weight-only quantization and (2) weight-activation quantization.

The weight-only quantization converts LLM weights to low-bit values. For example, GPTQ (Frantar et al., 2022) quantizes one column of a weight matrix while updating the remaining columns based on the second-order Hessian to compensate for the quantization error. AWQ (Lin et al., 2024) employs grid-searching to find the optimal scaling factor and clipping threshold that minimize the quantization error. OmniQuant (Shao et al., 2024) extends AWQ by learning the optimal weight clipping through block-wise backpropagation. In addition, these methods apply group-wise quantization (Dettmers et al., 2022) to further boost the model performance compared to channel-wise quantization. Our work also focuses on group-wise quantization, as it incurs minimal computational overhead (only a matrix reshape is required). Specifically, the tiny and compact encoding of RaZeR allows fine-grained datatype adaptation, which assigns a different special value to different weight groups to minimize the quantization error.

The weight-activation quantization compresses both weights and activations. For instance, SmoothQuant (Xiao et al., 2022) migrates the quantization difficulty from activations to weights through a mathematically equivalent transformation. On top of activation quantization, KV-cache quantization has recently received more traction since its memory footprint increases with higher batch sizes and longer input sequences (Yuan et al., 2024). Recent methods emphasize refining the granularity and direction of quantization to better handle the unique characteristics of tensor distribution in KV-Cache. For example, both Atom (Zhao et al., 2024) and FlexGen (Sheng et al., 2023) apply a group-wise asymmetric quantization approach, which groups contiguous KV-cache entries per token. Extending from this, recent works (Liu et al., 2024; Hooper et al., 2024) further explore the tensor distribution and propose a more refined strategy by quantizing the Key cache per channel to better capture the channel-wise outlier characteristics. To balance the storage overhead, KCVT (Kang et al., 2024) simplifies KIVI by removing fine-grained grouping.

3 MOTIVATION

In this section, we motivate RaZeR and provide our reasoning for selecting this numerical format. Specifically, we discuss both the efficiency and accuracy aspects of RaZeR relative to the two extremes of existing datatypes: integer and learned lookup tables.

Better Fit for LLM Distributions. The numerical distribu-

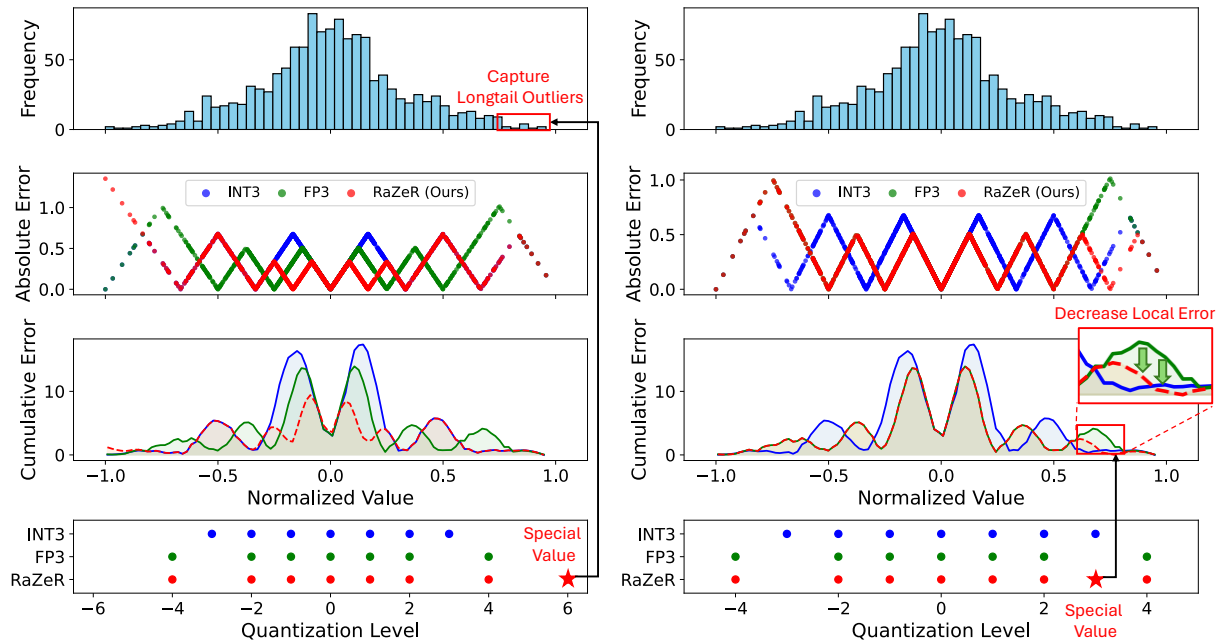


Figure 2. Numerical distribution and corresponding quantization error for quantizing a vector from the KV-Cache of Llama-3.2-3B using three datatypes. Compared to INT, FP decreases the error at the center of the distribution where there is the highest density of numbers, at the cost of higher error at the tail of the distribution. RaZeR further improves the FP datatype by remapping -0 to an additional “special value” thus decreasing the approximation error in its vicinity. In 3-bit RaZeR, one configuration (left) benefits more from extra range, while the other (right) benefits from additional resolution within the same range, both resulting in reduced overall quantization error.

tions in LLMs, and more generally neural networks, adhere to a long-tailed Normal distribution for both weights and activations (Dettmers et al., 2023; Dotzel et al., 2024; Kim et al., 2024). This is not a good match to the integer datatype that has uniformly-spaced quantization levels. As Figure 2 shows, INT quantization has higher absolute error at the center of the distribution where most numbers exist, leading to a higher cumulative error. The FP datatype reduces this error at the center of the distribution, at the expense of higher quantization error at the tail of the distribution. RaZeR alleviates this additional error by repurposing the negative zero encoding to an additional value that is optimized to decrease quantization error. This can be clearly seen in Figure 2, where the quantization error drops significantly in the lower two plots around the special value. Specifically, the left figure illustrates that introducing a special value outside the FP3 range can mitigate the quantization error associated with the asymmetric outlier tail of the Normal distribution. On the other hand, the right figure shows that adding a special value within the range of FP4 can also reduce the quantization error even if the Normal distribution is symmetric. Hence, combining the inherently well-suited FP datatype with this learnable special value can result in lower quantization error and superior accuracy when used in both weight and KV-cache quantization as we show in Section 5.

Compute-Capable Datatype. Compared to codebook or lookup table quantization, FP datatypes have the obvious advantage of being capable of performing computations as well. Furthermore, the latest GPUs (Nvidia B200 and AMD MI350X) support computations in FP4, making the investigation of LLM quantization for these datatypes practical and relevant for commodity hardware. However, the remapping of -0 in RaZeR is not supported by default, making these datatypes handicapped by just following the Open Compute Standard for floating-point numbers (Open Compute Project). Though out of scope of this paper, hardware support for RaZeR can be easily and cheaply added to existing GPU compute units. As we describe in Section 4, it is sufficient to limit the choices for the special value to just four options, making its storage and decoding easily achievable using four dedicated registers and a 4:1 multiplexer per TensorCore multiplier. Our work in this paper makes the case for and provides the empirical justification to support RaZeR for FP4 and FP3 datatypes. Furthermore, in Section 5 we describe how we implement a fast GPU kernel to achieve most of expected performance improvements using optimized bit manipulations to perform special value decoding.

Compact Encoding. The memory cost of storing quantization parameters becomes non-trivial for group-wise quantization (Dettmers et al., 2022). Table 1 summarizes the

Table 1. Comparison of encoding overhead between different methods at 4-bit group-wise quantization with a group size of 128.

Method	Work	Encoding	#Bits / Group	Eff. #Bits / Operand
INT4	GPTQ, AWQ OmniQuant	Scale factor;	8	4.09
		Zero point	4	
NF4	QLoRA	Scale factor	8	4.06
LUT	SqueezeLLM	LUT entry	256	6
RaZeR	Our Work	Scale factor;	8	4.08
		SV index	2	

encoding overhead of different methods for 4-bit group-wise quantization with a group size of 128. Conventional integer quantization stores an FP16 scaling factor and a 4-bit zero-point. The scaling factor can be further quantized to INT8 through double quantization (Dettmers et al., 2023), leading to an effective operand bit-width of 4.09. The custom datatype such as NF4 (Dettmers et al., 2023) only needs to store a scaling factor per group since the set of quantization values are fixed. SqueezeLLM (Kim et al., 2024) employs K-means clustering to find the optimal per-channel quantization values stored in a lookup table (LUT), which contains sixteen FP16 values. Unfortunately, it cannot be applied to group-wise quantization since the 256-bit encoding overhead leads to an extra $256/128 = 2$ bits per operand. On top of these methods, RaZeR strikes a reasonable balance between accuracy and encoding overhead. In addition to the scaling factor, RaZeR only stores 2-bit extra encoding per group, which is enough to encode the special values because we restrict its choice to just four possible options as described in Section 4.1. This constitutes a negligible 0.016-bit overhead per quantized operand.

4 METHODOLOGY

4.1 Problem Formulation

Our goal is to select a special value (sv) to improve the baseline datatype, FP4 or FP3 in our case, so that the quantization error ϵ_q is minimized.

$$sv = \arg \min_{sv} \epsilon_q \tag{4}$$

sv can be directly optimized by setting it as a trainable parameter and using backpropagation of either the activation quantization error (Shao et al., 2024) or the overall LLM loss during fine-tuning. However, this places no bounds on sv , and we found that practically, it is difficult to optimize sv directly in this way because of sparse gradient updates. Indeed, gradients only ever propagate to sv when it is selected by the $[\cdot]$ function in the quantization equation. We found that this makes sv optimization heavily dependent

on its initialization value. Furthermore, sv would often get stuck in a locally-optimal state such as one that aliases with existing quantized values.

Fundamentally, sv is limited to the range and values that are available in the computing numerical format. For example, if compute is to be done in FP16, then the sv can assume any FP16 value. However, using an arbitrary sv in FP16 incurs considerable encoding overhead for group-wise quantization. This is because RaZeR assigns a different sv to make the extended FP4/FP3 better adapt to the group distribution, leading to $16 / 128 = 0.125$ extra bits per operand for a group size of 128. This motivates a simpler problem formulation, in which sv is selected among a discrete set of empirically-determined candidate special values, denoted as SV . Consequently, the encoding overhead for identifying the per-group $sv \in SV$ becomes a $\log |SV|$ -bit index. We set $|SV|$ to contain 4 integer values in RaZeR, which not only incurs tiny encoding overhead, but also allows efficient dequantization as we will discuss in Section 4.4.

During quantization, we can iterate over SV and pick the one with the lowest ϵ_q . In addition to exhaustive search for sv , we can also perform a differentiable search to convert the discrete choice for sv for each group i into a softmax combination of all possible SV . Following prior work (Liu et al., 2019), this is weighted by learnable parameters α_{sv} , and modulated by softmax temperature τ that is annealed to zero during a calibration phase to select a single sv .

$$sv(i) = \sum_{sv \in SV} \frac{\exp(\frac{\alpha_{sv}^{(i)}}{\tau})}{\sum_{sv' \in SV} \exp(\frac{\alpha_{sv'}^{(i)}}{\tau})} sv \tag{5}$$

In practice, the differentiable search was indeed effective in optimizing the special value for weight quantization but was sensitive to fine-tuning hyperparameters, yielding mixed results across different LLMs. This motivates our relatively simpler methodology of exhaustively iterating over a special value set SV .

4.2 Special Value Set Calibration

Low bit-width limits the expressiveness of quantized tensors with respect to the original weight or KV-cache distribution. This makes it crucial to calibrate SV effectively for the distribution of each model. Given that SV are specific values that aim to reduce the quantization error, we propose a search strategy to find the best SV set from all possible sets by minimizing the per-layer output activation error as done by (Lin et al., 2024). However, the only constraint of SV is that it differs from the basic FP4/FP3 values, making the search space relatively unbounded. To address this challenge, for each model, we apply a simple heuristic to reduce the search space by quantifying the operand (weight or

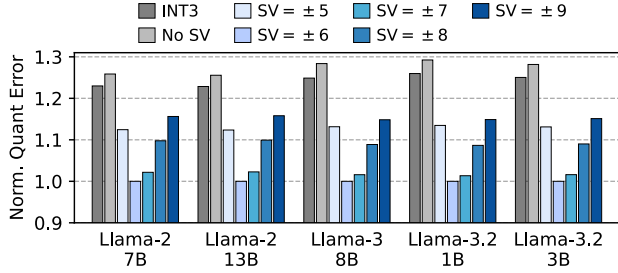


Figure 3. Normalized weight quantization error (\downarrow) with respect to different special values (SV) for FP3. We use group-wise quantization with a group size of 128.

KV-cache) quantization error with respect to an individual special value.

For example, Figure 3 shows the normalized error for group-wise quantization on different Llama models when using sv with different absolute values. Without using a special value, the basic FP3 datatype has a higher error than the asymmetric INT3 quantization. On the other hand, adding sv from ± 5 to ± 9 consistently achieves lower quantization error than INT3. Moreover, the error of adding sv consistently follows a parabolic shape, with the lowest error occurring around ± 6 and continuing to increase at a large absolute sv . Intuitively, a large sv indicates a very long-tailed distribution, which would distort the original FP3 quantization levels. Hence, the search space of SV does not need to contain values with a large absolute value. In this example, we can safely restrict the search space of sv to the interval $[-9, +9]$.

After determining the search space for each model, we search for a set of 4 special values using covariance matrix adaptation evolution strategy (CMA-ES) provided within Optuna (Akiba et al., 2019), with the objective of minimizing per-layer quantization error. Algorithm 1 shows the overall flow of our search. We find different per-layer SV for weights and KV-cache in lines 1–3 based on the search ranges $[sv_{\min}, sv_{\max}]$ determined empirically. Next, line 4 rounds SV to a provided number of bits. Practically, we have only needed 6 bits to store SV . Finally, there is

Algorithm 1: Special value set search.

Input : LLM with L layers, weights W_l and KV-cache KV_l for each layer l .

Output : Set of $S = 4$ special values for weights SV_{model}^W and KV-cache SV_{model}^{KV} for the entire model.

- 1 **for** each layer $l = 1, \dots, L$ **do**
- 2 $SV_l^W = \text{search}(W_l, [sv_{\min}^W, sv_{\max}^W])$
- 3 $SV_l^{KV} = \text{search}(KV_l, [sv_{\min}^{KV}, sv_{\max}^{KV}])$
- 4 $\{SV_l^W, SV_l^{KV}\}_{l=1}^L = \text{Round}(\{SV_l^W, SV_l^{KV}\}_{l=1}^L, \text{nbits})$
- 5 $\{SV_{\text{model}}^W, SV_{\text{model}}^{KV}\} = \text{Cluster}(\{SV_l^W, SV_l^{KV}\}_{l=1}^L, S)$

an *optional* clustering step to compress the per-layer SV to a single 4-entry LUT for the whole model. While this greatly limits the SV options compared to having a different SV per-layer, we found that this was already sufficient to outperform existing methods. Therefore, all our results use per-model SV and we leave the investigation of per-layer and other more granular SV to future work. The entire special value set search is practical and fast, needing only 50 calibrationsa samples from WikiText2 and taking ~ 7.5 minutes on an A6000 GPU for an 8B Llama model. Table 2 verifies our search-based SV calibration by showing improvements on both accuracy and perplexity compared to a manually-crafted $SV = \{-10, -5, +5, +10\}$ for FP4+RaZeR KV-cache quantization.

4.3 KV-Cache Quantization

We build on KV-cache quantization algorithms that use dynamic quantization to capture changing distributions. We employ a straightforward exhaustive search to determine the optimal sv that minimizes quantization MSE error. Given the relatively small size of SV , which can be calibrated in advance, this search incurs a bounded overhead of at most $|SV|$ times compared to basic quantization without special values. Although this adds some computational overhead, it remains practical due to the compact size of SV . To further reduce online quantization overhead, we implement a local buffering strategy (Liu et al., 2024; Kang et al., 2024). Newly generated tokens are temporarily stored in a small buffer at full precision, with quantization applied only once the buffer reaches its capacity, n_b . While this adds minor storage overhead, it significantly reduces the amortized computational cost per decoding step, effectively lowering the quantization overhead by a factor of $1/n_b$.

4.4 Encoding for Efficient GPU Acceleration

Even though FP4 support is coming to the newest GPUs, currently-available GPUs such as Nvidia H100 and AMD MI300X do not include either software or hardware support for the FP4 datatype. Furthermore, we have an additional special value processing for RaZeR that has to be performed. We therefore create an efficient CUDA kernel to perform fast casting from RaZeR to FP16, achieving a $5\times$ speedup compared to naively performing a 16-way lookup for all possible values of 4-bit RaZeR. This is integrated within our

Table 2. SV calibration improves perplexity and accuracy compared to a manually-crafted SV .

Task	Llama-3-8B	Llama-3.2-3B
GSM8K – ACC (\uparrow)	+ 0.23	+ 1.37
Wikitext2 – PPL (\downarrow)	– 0.02	– 0.04

Table 3. Modified RaZeR FP4 encoding to enable fast casting to FP16 on currently-available GPU devices.

Decimal	FP4 E2M1	FP16 Binary			RaZeR
	{S, E, M}	S	E	M ₁₀	{E, M, S}
0.0	0000	0	00000	0	0010
0.5	0001	0	01110	0	0000
1.0	0010	0	01111	1	0100
1.5	0011	0	01111	1	0110
2.0	0100	0	10000	0	1000
3.0	0101	0	10000	1	1010
4.0	0110	0	10001	0	1100
6.0	0111	0	10001	1	1110
<i>sv</i>	1000	1	01110	1	1000

fast matrix multiplication kernels that are further evaluated in Section 5.4. However, a specific encoding scheme shown in Table 3 is needed for our optimized kernel.

FP4 (E2M1) and FP16 (E5M10) have similar structure, both have the sign, exponent, mantissa bits. To move the sign bit from the 4th position in FP4 to the 16th position in FP16, a bit mask can pick the sign bit, and a left shift operation can get it to the correct position. We encode the FP4 sign bit at the end of FP4, in the zeroth bit instead of the third bit (as shown in Table 3) to avoid the masking operation and only perform a shift-by-15 (line 3 in Listing 1)

FP16 exponents only differ from FP4 exponents in the exponent bias value, therefore, we simply add the difference between the two exponent biases and left shift by 8 to move to the correct bit positions (line 5) after extracting *both* the exponent and mantissa from the FP4 number through masking (line 4). Note that we can process the exponent and mantissa together because the single mantissa bit in FP4 does not need to change except in two special cases for subnormals: 0.5 as ‘0001’, and 0 as ‘0000’. For 0.5 (0001), the 10th mantissa is not same as the the mantissa of original FP4 mantissa because 0.5 in FP16 is not a denormalized number anymore. To avoid special-casing subnormals using if-statements, we remap the 0.5 value to 0000 (as shown in Table 3) so that its mantissa value will not need to be changed after shifting.

Since there are only 4 special values in our RaZeR methodology, we use a small look-up table (line 9) to select the correct one. Finally, we compare with the FP16 encodings of -0 and $+0$ to determine if we should use the special value (line 13) or replace with zero value (line 14). We pack four FP4 numbers in a single INT32 datatype to ensure efficient GPU memory access. By performing the comparisons on lines 13-14 in the FP16 domain, we conserve an additional mask operation that would’ve been required to extract the FP4 number from its INT32 container. The FP3 format employs dual 128-bit sets—one for sign bits and two for exponent bits—to encode weight groups. This structure en-

Listing 1. Pseudo-code for efficient type conversion from FP4+RaZeR to FP16, used on current GPUs.

```

1 half fp42half(x, sv_idx):
2   // cast FP16 -> FP4
3   sign_fp16 = x << 15
4   Exp_Man_fp4 = x & 0xE
5   EM_fp16 = (0x38 + Exp_Man_fp4) << 8
6   V_fp = (sign_fp16 | EM_fp16)
7
8   // look-up special value
9   SVs[4] = {0x4500, 0x4800, 0xC500, 0xC800}
10  V_sv = SVs[sv_idx]
11
12  // select between {V_fp, V_sv, 0}
13  V = (V_fp == 0xBA00) ? V_sv : V_fp
14  V = (V_fp == 0x3A00) ? 0 : V
15
16  return _ushort_as_half(V)

```

ables efficient CUDA processing via float4/uint4 operations, and zero memory waste overhead.

5 EXPERIMENTS

5.1 Settings

Quantization Setup. We conduct experiments on both weight-only and KV-cache quantization at 4-bit and 3-bit precision. We adopt group-wise quantization since it always provides a better trade-off between model size and performance (Dettmers et al., 2022). Following prior works (Lin et al., 2024; Shao et al., 2024; Kang et al., 2024), we use a group size of 128 and 64 for weight and KV-cache quantization, respectively throughout our evaluation, unless otherwise specified.

Models and Datasets. We benchmark RaZeR on popular open-sourced Llama-2, Llama-3, and Llama-3.2 models (Touvron et al., 2023; Meta AI, a;b). For weight-only quantization, we focus on evaluating the perplexity on WikiText2 (Merity et al., 2016) and C4 (Dodge et al., 2021) datasets since perplexity can stably reflect the LLM performance (Dettmers & Zettlemoyer, 2022). We also evaluate the zero-shot accuracy on PIQA (Bisk et al., 2019), ARC (Clark et al., 2018), BoolQ (Clark et al., 2019), HellaSwag (Zellers et al., 2019), and WinoGrande (Sakaguchi et al., 2019) using lm-evaluation harness (Gao et al., 2023). For KV-cache quantization, we measure exact-match accuracy on the GSM8K (Cobbe et al., 2021) datasets for complex math reasoning, both with and without chain-of-thought (CoT) prompting (Wei et al., 2023).

Baselines. To demonstrate the benefits of RaZeR over conventional asymmetric integer quantization, we combine RaZeR with recent weight-only quantization methods AWQ (Lin et al., 2024) and OmniQuant (Shao et al., 2024), in addition to KV-cache quantization methods KCVT (Kang et al., 2024) and KIVI (Liu et al., 2024). We use the official github code of these works to reproduce their results, and

Table 4. Perplexity (\downarrow) of weight-only quantized Llama models, context length 2048.

#Bits	Method	Wikitext2 PPL (\downarrow)							C4 PPL (\downarrow)						
		2-7B	2-13B	2-70B	3-8B	3-70B	3.2-1B	3.2-3B	2-7B	2-13B	2-70B	3-8B	3-70B	3.2-1B	3.2-3B
16	FP16	5.47	4.88	3.32	6.14	2.85	9.75	7.81	6.97	6.47	5.52	8.88	6.73	12.72	10.43
w4g128	INT4-Asym	5.73	4.98	3.46	6.73	3.71	11.72	8.49	7.25	6.59	5.63	9.64	7.94	15.55	11.44
	FP4	5.70	5.02	3.46	6.74	3.52	11.29	8.48	7.23	6.61	5.62	9.65	7.66	14.93	11.38
	\downarrow w/ RaZeR	5.67	4.99	3.43	6.63	3.35	10.99	8.30	7.19	6.58	5.61	9.50	7.55	14.43	11.17
	AWQ	5.60	4.97	3.41	6.55	3.24	10.83	8.23	7.12	6.56	5.58	9.41	6.97	14.13	11.08
	\downarrow w/ RaZeR	5.59	4.96	3.40	6.50	3.19	10.59	8.17	7.09	6.55	5.57	9.32	6.94	13.84	10.97
	OmniQuant	5.59	4.96	–	6.57	–	10.72	8.24	7.12	6.57	–	9.50	–	14.19	11.13
	\downarrow w/ RaZeR	5.56	4.95	–	6.45	–	10.39	8.07	7.06	6.55	–	9.34	–	13.80	10.95
w3g128	INT3-Asym	6.66	5.52	3.98	12.07	10.65	34.80	13.22	8.41	7.18	6.02	16.45	19.14	44.92	17.03
	FP3	6.89	5.67	4.11	13.48	10.21	51.69	16.01	8.72	7.31	6.12	17.85	16.92	63.07	18.89
	\downarrow w/ RaZeR	6.27	5.38	3.85	8.46	8.57	19.50	11.21	7.90	7.00	5.90	11.99	14.69	25.36	14.75
	AWQ	6.24	5.32	3.73	8.15	4.66	16.63	10.31	7.81	6.95	5.81	11.49	7.87	21.09	13.82
	\downarrow w/ RaZeR	6.07	5.27	3.70	7.79	4.48	14.86	9.83	7.64	6.88	5.77	11.07	7.76	18.81	13.16
	OmniQuant	6.05	5.28	–	8.33	–	15.64	10.12	7.76	6.99	–	12.04	–	21.37	14.03
	\downarrow w/ RaZeR	5.86	5.17	–	7.56	–	12.85	9.09	7.55	6.84	–	11.06	–	17.87	12.84

Table 5. Zero-shot accuracy (\uparrow) of weight-only quantized Llama-3 and Llama-3.2 models.

Model	#Bits	Method	Zero-shot Accuracy (\uparrow)						
			PIQA	ARC-e	ARC-c	BoolQ	Hella	Wino	Average
3-8B	16	FP16	79.65	80.09	50.43	60.2	72.53	81.31	70.7
		AWQ	79.38	79.67	49.74	59.35	72.85	79.72	70.12
		\downarrow w/ RaZeR	79.49	79.34	48.98	59.29	72.93	81.07	70.18
	w4g128	OmniQuant	78.73	80.05	49.83	59.41	72.85	79.51	70.06
		\downarrow w/ RaZeR	79.49	80.26	50.09	59.11	72.61	78.20	69.96
		AWQ	77.64	75.67	44.03	55.35	71.43	78.32	67.07
	w3g128	\downarrow w/ RaZeR	77.20	77.86	46.16	56.70	71.35	78.93	68.03
		OmniQuant	76.33	69.49	40.10	55.08	69.30	74.22	64.09
		\downarrow w/ RaZeR	77.42	76.14	44.62	56.64	69.69	73.09	66.27
3.2-1B	16	FP16	74.43	65.36	31.31	47.73	60.85	63.98	57.28
		AWQ	73.67	63.43	30.38	46.25	59.59	64.25	56.26
		\downarrow w/ RaZeR	73.99	64.23	32.59	46.50	60.54	61.80	56.61
	w4g128	OmniQuant	73.34	62.67	29.86	46.32	58.25	61.8	55.37
		\downarrow w/ RaZeR	73.99	64.14	29.86	46.52	59.51	63.09	56.19
		AWQ	69.53	55.56	27.56	41.44	55.49	60.58	51.69
	w3g128	\downarrow w/ RaZeR	71.44	59.26	27.56	42.11	56.67	62.14	53.20
		OmniQuant	68.82	56.27	25.43	40.22	54.93	54.53	50.03
		\downarrow w/ RaZeR	71.00	58.46	28.33	42.20	55.33	58.32	52.27
3.2-3B	16	FP16	76.61	74.54	42.15	55.32	69.77	73.21	65.27
		AWQ	76.77	72.77	40.78	54.37	69.22	72.11	64.34
		\downarrow w/ RaZeR	76.99	72.98	40.70	54.48	68.98	75.02	64.86
	w4g128	OmniQuant	76.99	73.11	41.81	54.41	67.32	70.61	64.04
		\downarrow w/ RaZeR	76.28	72.94	40.96	54.35	67.96	68.96	63.57
		AWQ	73.81	68.48	37.54	50.24	66.46	71.47	61.33
	w3g128	\downarrow w/ RaZeR	73.94	70.50	37.37	50.96	66.06	72.08	61.82
		OmniQuant	74.05	66.88	34.04	49.61	65.11	68.26	59.66
		\downarrow w/ RaZeR	76.12	71.21	37.12	51.53	66.54	70.21	62.12

Table 6. Perplexity (\downarrow) of KV-cache quantization

Method	#Bits	Wikitext2 PPL			
		2-8B	2-13B	3-8B	3.2-3B
FP16	16	5.47	4.88	6.14	7.81
KTVT	4	5.57	4.95	6.38	8.24
↳ w/ RaZeR	4	5.57	4.97	6.41	8.26
KCVT	4	5.65	5.12	6.47	8.24
↳ w/ RaZeR	4	5.60	5.00	6.38	8.09
KIVI	4	5.49	4.90	6.20	7.95
↳ w/ RaZeR	4	5.50	4.90	6.21	7.90
KTVT	3	6.12	5.32	7.89	12.93
↳ w/ RaZeR	3	5.98	5.21	7.32	10.66
KCVT	3	7.07	7.33	7.37	12.70
↳ w/ RaZeR	3	6.40	5.80	7.31	9.15
KIVI	3	5.57	4.96	6.43	8.22
↳ w/ RaZeR	3	5.55	4.95	6.38	8.16

we replace their original asymmetric integer quantizer with a non-uniform quantizer that maps FP16 values to RaZeR.

5.2 Results on Weight-only Quantization

Perplexity. Table 4 reports the perplexity results of different quantization methods. As the table shows, RaZeR consistently outperforms the asymmetric integer quantization with and without advanced optimization techniques, i.e., AWQ and OmniQuant. These findings suggest the versatility of RaZeR, being adaptable to a multitude of quantization configurations and strategies. Furthermore, the performance improvement of RaZeR becomes more pronounced for 3-bit precision and smaller models such as the Llama-3.2 variants.

Zero-shot Accuracy. Table 5 reports the zero-shot accuracy of six downstream tasks. In most cases, combining RaZeR with AWQ and OmniQuant achieves better accuracy than using the conventional asymmetric integer datatypes. For example, in 3-bit quantization, RaZeR increases the average accuracy of AWQ and OmniQuant by 0.94% and 2.18%, respectively, on Llama-3-8B.

5.3 Results on KV-Cache Quantization

Perplexity. Table 6 presents the perplexity evaluation results for various KV-Cache quantization methods. As with the improvements observed when combining RaZeR with weight-only quantization, RaZeR consistently reduces perplexity when applied alongside off-the-shelf KV-Cache quantization methods. For example, in the 3-bit quantization setting, RaZeR significantly reduces the perplexity of KCVT by 3.55 on the Llama-3.2-3B model, demonstrating RaZeR’s ability to better capture the tensor distribution.

Table 7. Accuracy (\uparrow) of KV-cache quantization on GSM8K.

Method	#Bits	Llama-3-8b		Llama-3.2-3b	
		w/o CoT	CoT	w/o CoT	CoT
FP16	16	50.04	52.39	64.14	76.95
Per-Token	4	46.39	47.76	60.57	73.99
↳ w/ RaZeR	4	44.12	48.60	62.47	71.87
KCVT	4	43.44	47.08	58.91	72.48
↳ w/ RaZeR	4	46.17	49.05	60.27	74.22
KIVI	4	48.45	52.76	61.71	76.19
↳ w/ RaZeR	4	49.20	51.70	62.85	77.79
Per-Token	3	26.61	25.92	24.56	45.94
↳ w/ RaZeR	3	29.19	33.66	32.97	57.24
KCVT	3	21.76	26.84	15.09	32.52
↳ w/ RaZeR	3	35.63	34.34	50.19	65.66
KIVI	3	44.81	46.32	59.36	73.62
↳ w/ RaZeR	3	47.08	49.96	60.96	74.37

Math Tasks. To further assess the performance of RaZeR on tasks requiring complex reasoning, we benchmarked it on GSM8K (Cobbe et al., 2021), a dataset comprised of mathematical problems that demand multistep solutions. As seen in Table 6, incorporating RaZeR into various KV-Cache quantization methods leads to a notable increase in accuracy. Notably, under the 3-bit quantization setting, RaZeR improves the accuracy of KIVI by up to 3.64% on the Llama-3-8B model, using chain-of-thought (CoT) prompting (Wei et al., 2023).

5.4 Inference Speed Evaluation

Settings. To evaluate the end-to-end performance of RaZeR, we use a batch size = 1 and follow the methodology of previous work (Lin et al., 2024), which uses a fixed prompt length of 6 tokens and generates 200 tokens to calculate the median latency as the final inference speed. We compare the kernel efficiency between RaZeR and Marlin (Frantar et al., 2024) on NVIDIA RTX 4090 and A6000 GPUs using the HuggingFace library’s Llama implementation. While previous works have developed other kernel optimization techniques such as operator fusion (Lin et al., 2024) and FlashAttention (Dao, 2023), they are universally orthogonal to other quantization kernels including RaZeR.

End-to-end Throughput. Figure 4 shows that RaZeR achieves comparable inference speed as Marlin, and offers up to $2.72\times$ speedup compared to the FP16 implementation. The higher speedup mainly occurs in large models that require significant memory and computation. Notably, for small models such as Llama-3.2-1B, where the GPU utilization becomes very low, Marlin achieves almost the

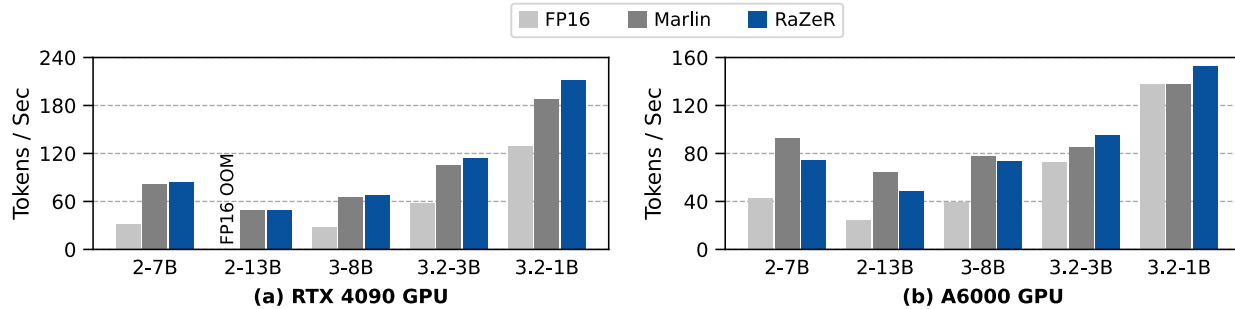


Figure 4. End-to-end throughput of RaZeR compared to FP16 and Marlin.

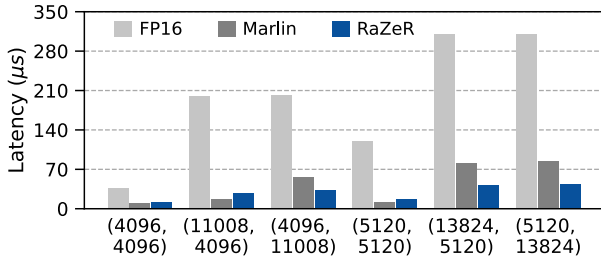


Figure 5. GEMV latency on RTX 4090. We compare the latency for linear layers of Llama-2 models. The horizontal-axis labels represent the weight matrix size in different linear layers.

same inference speed as FP16, while RaZeR still provides $1.11\times$ higher throughput compared to FP16.

GEMV Speedup. Figure 5 shows the GEMV latency on RTX 4090 GPU for different linear layers of Llama-2 models. Notably, RaZeR achieves up to $7.56\times$ speedup compared to the FP16 implementation. This happens because for large weight matrix such as 13824×5120 , the FP16 implementation needs 135 MB memory, which is larger than the available L2 cache with a size of 72 MB. Hence, the FP16 weight matrix will be partitioned and accessed multiple times from DRAM. Conversely, RaZeR compresses the weight to 4-bit, leading to a matrix capacity of only 33.75 MB, which can be fully stored in the L2 cache for faster access compared to DRAM.

6 DISCUSSION

In this implementation of RaZeR, we use FP4 as a storage datatype and cast to FP16 for compute as it is common in other works (Lin et al., 2024; Shao et al., 2024; Liu et al., 2024). This alleviates the memory bottleneck that limits performance in low-batch LLM inference. However, high batch inference with 4-bit weights and KV-cache can become compute-bound (Zhu et al., 2024), making it advantageous and more efficient to perform computations in low bit-width as well. RaZeR is very friendly and efficient for such computations due to its ultra compact special value lookup table, and its conformance with general floating-point compute. To process the special value in future GPU

hardware, an extra bit can simply be used for processing that value such that, for example, FP3 can be upcast to FP4 on the fly at the Tensorcore level. Alternatively, future GPU hardware can be designed to be more flexible in supporting mixed-precision. We have shown in prior work, that indeed, bit-serial computing can be one method to seamlessly integrate mixed-precision computing within MAC units and potentially GPU Tensorcores as well (Chen et al., 2025). This more flexible compute would also be advantageous for different quantization configurations. For example, it is often the case that LLM activations need to remain in 8-bits or higher for reasonable accuracy (Zhao et al., 2024; Lin* et al., 2024). Mixed 4-bit \times 8-bit multiply-accumulate operations would greatly benefit this common case if GPUs were to develop this capability.

7 CONCLUSION

In this paper, we propose RaZeR, a new datatype that repurposes the negative zero encoding of FP4/FP3 with a set of special values optimized to reduce quantization error. On the algorithm side, we propose a search strategy to find the optimal set of special values for each model while incurring tiny encoding overhead. By integrating RaZeR with state-of-the-art weight and KV-cache quantization methods, we demonstrate that employing RaZeR further improves the model performance across diverse language generation and zero-shot tasks, suggesting RaZeR’s adaptability to a multitude of quantization configurations and strategies. On the system side, we show that RaZeR can be efficiently accelerated on commodity GPUs through an efficient mixed-precision CUDA kernel, achieving up to $2.72\times$ higher decoding throughput compared to the FP16 baseline. With FP4/FP3 being widely supported by recently released GPUs, we believe that incorporating the hardware-friendly RaZeR datatype is highly valuable.

REFERENCES

- Akiba, T., Sano, S., Yanase, T., Ohta, T., and Koyama, M. Optuna: A next-generation hyperparameter optimization framework. In *Proceedings of the 25th ACM SIGKDD International Conference on Knowledge Discovery & Data Mining, KDD '19*, pp. 2623–2631, New York, NY, USA, 2019. Association for Computing Machinery. ISBN 9781450362016. doi: 10.1145/3292500.3330701. URL <https://doi.org/10.1145/3292500.3330701>.
- AMD. AMD Instinct MI350. URL <https://www.amd.com/en/newsroom/press-releases/2024-6-2-amd-accelerates-pace-of-data-center-ai-innovation-.html>.
- Bisk, Y., Zellers, R., Bras, R. L., Gao, J., and Choi, Y. PIQA: Reasoning about physical commonsense in natural language. *arXiv preprint arXiv:1911.11641*, 2019.
- Chee, J., Cai, Y., Kuleshov, V., and Sa, C. D. QuIP: 2-bit quantization of large language models with guarantees. In *Thirty-seventh Conference on Neural Information Processing Systems*, 2023.
- Chen, M., Shao, W., Xu, P., Wang, J., Gao, P., Zhang, K.-C., Qiao, Y., and Luo, P. EfficientQAT: Efficient quantization-aware training for large language models. *arXiv preprint arXiv:2407.11062*, 2024.
- Chen, Y., AbouElhamayed, A. F., Dai, X., Wang, Y., Andronic, M., Constantinides, G. A., and Abdelfattah, M. S. Bitmod: Bit-serial mixture-of-datatype llm acceleration. In *IEEE International Symposium on High-Performance Computer Architecture (HPCA)*, 2025.
- Choi, J., Wang, Z., Venkataramani, S., Chuang, P. I.-J., Srinivasan, V., and Gopalakrishnan, K. Pact: Parameterized clipping activation for quantized neural networks. *arXiv preprint arXiv:1805.06085*, 2018.
- Clark, C., Lee, K., Chang, M.-W., Kwiatkowski, T., Collins, M., and Toutanova, K. BoolQ: Exploring the surprising difficulty of natural yes/no questions. *arXiv preprint arXiv:1905.10044*, 2019.
- Clark, P., Cowhey, I., Etzioni, O., Khot, T., Sabharwal, A., Schoenick, C., and Tafjord, O. Think you have solved question answering? try ARC, the ai2 reasoning challenge. *arXiv preprint arXiv:1803.05457*, 2018.
- Cobbe, K., Kosaraju, V., Bavarian, M., Chen, M., Jun, H., Kaiser, L., Plappert, M., Tworek, J., Hilton, J., Nakano, R., Hesse, C., and Schulman, J. Training verifiers to solve math word problems. *arXiv preprint arXiv:2110.14168*, 2021.
- Dao, T. FlashAttention-2: Faster attention with better parallelism and work partitioning. *arXiv preprint arXiv:2307.08691*, 2023.
- Dettmers, T. and Zettlemoyer, L. The case for 4-bit precision: k-bit inference scaling laws. In *International Conference on Machine Learning*, 2022.
- Dettmers, T., Lewis, M., Shleifer, S., and Zettlemoyer, L. 8-bit optimizers via block-wise quantization. *arXiv preprint arXiv:2110.02861*, 2022.
- Dettmers, T., Pagnoni, A., Holtzman, A., and Zettlemoyer, L. QLoRA: Efficient finetuning of quantized LLMs. In *Thirty-seventh Conference on Neural Information Processing Systems*, 2023.
- Dettmers, T., Lewis, M., Belkada, Y., and Zettlemoyer, L. Llm.int8(): 8-bit matrix multiplication for transformers at scale. In *Proceedings of the 36th International Conference on Neural Information Processing Systems*, 2024.
- Dodge, J., Marasovic, A., Ilharco, G., Groeneveld, D., Mitchell, M., and Gardner, M. Documenting large web-text corpora: A case study on the colossal clean crawled corpus. In *Conference on Empirical Methods in Natural Language Processing (EMNLP)*, 2021.
- Dotzel, J., Chen, Y., Kotb, B., Prasad, S., Wu, G., Li, S., Abdelfattah, M. S., and Zhang, Z. Learning from students: Applying t-distributions to explore accurate and efficient formats for LLMs. In *Forty-first International Conference on Machine Learning*, 2024.
- Frantar, E., Ashkboos, S., Hoefler, T., and Alistarh, D. Gptq: Accurate post-training quantization for generative pre-trained transformers. *arXiv preprint arXiv:2210.17323*, 2022.
- Frantar, E., Castro, R. L., Chen, J., Hoefler, T., and Alistarh, D. MARLIN: Mixed-precision auto-regressive parallel inference on large language models. *arXiv preprint arXiv:2408.11743*, 2024.
- Gao, L., Tow, J., Abbasi, B., Biderman, S., Black, S., DiPofi, A., Foster, C., Golding, L., Hsu, J., Le Noac’h, A., Li, H., McDonnell, K., Muennighoff, N., Ociepa, C., Phang, J., Reynolds, L., Schoelkopf, H., Skowron, A., Sutawika, L., Tang, E., Thite, A., Wang, B., Wang, K., and Zou, A. A framework for few-shot language model evaluation, 12 2023. URL <https://zenodo.org/records/10256836>.
- Guo, D., Zhu, Q., Yang, D., Xie, Z., Dong, K., Zhang, W., Chen, G., Bi, X., Wu, Y., Li, Y. K., Luo, F., Xiong, Y., and Liang, W. DeepSeek-Coder: When the large language model meets programming - the rise of code intelligence. *arXiv preprint arXiv:2401.14196*, 2024a.

- Guo, H., Brandon, W., Cholakov, R., Ragan-Kelley, J., Xing, E. P., and Kim, Y. Fast matrix multiplications for lookup table-quantized llms. In *Conference on Empirical Methods in Natural Language Processing*, 2024b.
- Hooper, C., Kim, S., Mohammadzadeh, H., Mahoney, M. W., Shao, Y. S., Keutzer, K., and Gholami, A. Kvquant: Towards 10 million context length llm inference with kv cache quantization. *arXiv preprint arXiv:2401.18079*, 2024.
- Hui, B., Yang, J., Cui, Z., Yang, J., Liu, D., Zhang, L., Liu, T., Zhang, J., Yu, B., Dang, K., Yang, A., Men, R., Huang, F., Ren, X., Ren, X., Zhou, J., and Lin, J. Qwen2.5-Coder technical report. *arXiv preprint arXiv:2409.12186*, 2024.
- Kang, H., Zhang, Q., Kundu, S., Jeong, G., Liu, Z., Krishna, T., and Zhao, T. GEAR: An efficient kv cache compression recipe for near-lossless generative inference of llm. *arXiv preprint arXiv:2403.05527*, 2024.
- Kim, S., Hooper, C., Gholami, A., Dong, Z., Li, X., Shen, S., Mahoney, M. W., and Keutzer, K. SqueezeLLM: Dense-and-sparse quantization. In *Forty-first International Conference on Machine Learning*, 2024.
- Lin, J., Tang, J., Tang, H., Yang, S., Chen, W.-M., Wang, W.-C., Xiao, G., Dang, X., Gan, C., and Han, S. Awq: Activation-aware weight quantization for llm compression and acceleration. In *Proceedings of Machine Learning and Systems (MLSys)*, 2024.
- Lin*, Y., Tang*, H., Yang*, S., Zhang, Z., Xiao, G., Gan, C., and Han, S. Qserve: W4a8kv4 quantization and system co-design for efficient llm serving. *arXiv preprint arXiv:2405.04532*, 2024.
- Liu, H., Simonyan, K., and Yang, Y. DARTS: Differentiable architecture search. In *International Conference on Learning Representations*, 2019.
- Liu, Z., Yuan, J., Jin, H., Zhong, S., Xu, Z., Braverman, V., Chen, B., and Hu, X. Kivi: A tuning-free asymmetric 2bit quantization for kv cache. *arXiv preprint arXiv:2402.02750*, 2024.
- Merity, S., Xiong, C., Bradbury, J., and Socher, R. Pointer sentinel mixture models. *arXiv preprint arXiv:1609.07843*, 2016.
- Meta AI. LIntroducing Meta Llama 3: The most capable openly available LLM to date, a. URL <https://ai.meta.com/blog/meta-llama-3/>.
- Meta AI. Llama 3.2: Revolutionizing edge AI and vision with open, customizable models, b. URL <https://ai.meta.com/blog/llama-3-2-connect-2024-vision-edge-mobile-devices/>.
- NVIDIA. NVIDIA GB200 NVL72, a. URL <https://www.nvidia.com/en-us/data-center/gb200-nvl72/>.
- NVIDIA. NVIDIA HGX AI Supercomputer, b. URL <https://www.nvidia.com/en-us/data-center/hgx/>.
- Open Compute Project. OCP Microscaling Formats (MX) Specification. URL <https://www.opencompute.org/documents/ocp-microscaling-formats-mx-v1-0-spec-final-pdf>.
- OpenAI. Introducing ChatGPT. URL <https://openai.com/index/chatgpt/>.
- Sakaguchi, K., Bras, R. L., Bhagavatula, C., and Choi, Y. WinoGrande: An adversarial winograd schema challenge at scale. *arXiv preprint arXiv:1907.10641*, 2019.
- Shao, W., Chen, M., Zhang, Z., Xu, P., Zhao, L., Li, Z., Zhang, K., Gao, P., Qiao, Y., and Luo, P. Omniquant: Omnidirectionally calibrated quantization for large language models. In *The Twelfth International Conference on Learning Representations*, 2024.
- Sheng, Y., Zheng, L., Yuan, B., Li, Z., Ryabinin, M., Fu, D. Y., Xie, Z., Chen, B., Barrett, C., Gonzalez, J. E., Liang, P., Ré, C., Stoica, I., and Zhang, C. Flexgen: High-throughput generative inference of large language models with a single gpu, 2023. URL <https://arxiv.org/abs/2303.06865>.
- Touvron, H., Martin, L., Stone, K. R., Albert, P., Almahairi, A., Babaei, Y., Bashlykov, N., Batra, S., Bhargava, P., Bhosale, S., Bikel, D. M., Blecher, L., Ferrer, C. C., Chen, M., Cucurull, G., Esiobu, D., Fernandes, J., Fu, J., Fu, W., Fuller, B., Gao, C., Goswami, V., Goyal, N., Hartshorn, A. S., Hosseini, S., Hou, R., Inan, H., Kardas, M., Kerkez, V., Khabsa, M., Kloumann, I. M., Korenev, A. V., Koura, P. S., Lachaux, M.-A., Lavril, T., Lee, J., Liskovich, D., Lu, Y., Mao, Y., Martinet, X., Mihaylov, T., Mishra, P., Molybog, I., Nie, Y., Poulton, A., Reizenstein, J., Rungta, R., Saladi, K., Schelten, A., Silva, R., Smith, E. M., Subramanian, R., Tan, X., Tang, B., Taylor, R., Williams, A., Kuan, J. X., Xu, P., Yan, Z., Zarov, I., Zhang, Y., Fan, A., Kambadur, M., Narang, S., Rodriguez, A., Stojnic, R., Edunov, S., and Scialom, T. Llama 2: Open foundation and fine-tuned chat models. *arXiv preprint arXiv:2307.09288*, 2023.
- Tseng, A., Chee, J., Sun, Q., Kuleshov, V., and Sa, C. D. QuIPs\\$: Even better LLM quantization with hadamard incoherence and lattice codebooks. In *Forty-first International Conference on Machine Learning*, 2024.

- Wei, J., Wang, X., Schuurmans, D., Bosma, M., Ichter, B., Xia, F., Chi, E., Le, Q., and Zhou, D. Chain-of-thought prompting elicits reasoning in large language models. *arXiv preprint arXiv:2201.11903*, 2023.
- Wu, H., Judd, P., Zhang, X., Isaev, M., and Micikevicius, P. Integer quantization for deep learning inference: Principles and empirical evaluation. *arXiv preprint arXiv:2004.09602*, 2020.
- Wu, Q., Bansal, G., Zhang, J., Wu, Y., Li, B., Zhu, E., Jiang, L., Zhang, X., Zhang, S., Liu, J., Awadallah, A. H., White, R. W., Burger, D., and Wang, C. AutoGen: Enabling next-gen llm applications via multi-agent conversation. *arXiv preprint arXiv:2308.08155*, 2023.
- Xiao, G., Lin, J., Seznec, M., Demouth, J., and Han, S. SmoothQuant: Accurate and efficient post-training quantization for large language models. *arXiv preprint arXiv:2211.10438*, 2022.
- Yuan, Z., Shang, Y., Zhou, Y., Dong, Z., Xue, C., Wu, B., Li, Z., Gu, Q., Lee, Y. J., Yan, Y., Chen, B., Sun, G., and Keutzer, K. LLM inference unveiled: Survey and roofline model insights. *arXiv preprint arXiv:2402.16363*, 2024.
- Zellers, R., Holtzman, A., Bisk, Y., Farhadi, A., and Choi, Y. HellaSwag: Can a machine really finish your sentence? In *Annual Meeting of the Association for Computational Linguistics (ACL)*, 2019.
- Zhao, Y., Lin, C.-Y., Zhu, K., Ye, Z., Chen, L., Zheng, S., Ceze, L., Krishnamurthy, A., Chen, T., and Kasikci, B. Atom: Low-bit quantization for efficient and accurate llm serving. In *Proceedings of Machine Learning and Systems (MLSys)*, 2024.
- Zhu, K., Zhao, Y., Zhao, L., Zuo, G., Gu, Y., Xie, D., Gao, Y., Xu, Q., Tang, T., Ye, Z., Kamahori, K., Lin, C.-Y., Wang, S., Krishnamurthy, A., and Kasikci, B. Nanoflow: Towards optimal large language model serving throughput. *arXiv preprint arXiv:2408.12757*, 2024.